Monthly Notices of the ROYAL ASTRONOMICAL SOCIETY

MNRAS **450,** 3966–3974 (2015) doi:10.1093/mnras/stv889

A double white dwarf with a paradoxical origin?

M. C. P. Bours,[1⋆] T. R. Marsh,[1] B. T. Gänsicke,[1] T. M. Tauris,[2,3] A. G. Istrate,[2] C. Badenes,[4] V. S. Dhillon,[5] A. Gal-Yam,[6] J. J. Hermes,[1] S. Kengkriangkrai,[7] M. Kilic,[8] D. Koester,[9] F. Mullally,[10] N. Prasert,[7] D. Steeghs,[1] S. E. Thompson[10] and J. R. Thorstensen[11]

[1]*Department of Physics, University of Warwick, Coventry CV4 7AL, UK*
[2]*Argelander-Institut für Astronomie, Universität Bonn, Auf dem Hügel 71, D-53121 Bonn, Germany*
[3]*Max-Planck-Institut für Radioastronomie, Auf dem Hügel 69, D-53121 Bonn, Germany*
[4]*Department of Physics and Astronomy, University of Pittsburgh, Allen Hall, 3941 O'Hara St, Pittsburgh, PA 15260, USA*
[5]*Department of Physics and Astronomy, University of Sheffield, Sheffield S3 7RH, UK*
[6]*Department of Particle Physics and Astrophysics, Weizmann Institute of Science, 76100 Rehovot, Israel*
[7]*National Astronomical Research Institute of Thailand, 191 Siripphanich Building, Huay Kaew Road, Chiang Mai 50200, Thailand*
[8]*Department of Physics and Astronomy, University of Oklahoma, 440 W. Brooks St, Norman, OK 73019, USA*
[9]*Institut für Theoretische Physik und Astrophysik, Universität Kiel, D-24098 Kiel, Germany*
[10]*SETI Institute/NASA Ames Research Center, Moffet Field, CA 94035, USA*
[11]*Department of Physics and Astronomy, Dartmouth College, Hanover, NH 03755, USA*

Accepted 2015 April 18. Received 2015 April 14; in original form 2015 March 27

ABSTRACT

We present *Hubble Space Telescope* UV spectra of the 4.6-h-period double white dwarf SDSS J125733.63+542850.5. Combined with Sloan Digital Sky Survey optical data, these reveal that the massive white dwarf (secondary) has an effective temperature $T_2 = 13\,030 \pm 70 \pm 150$ K and a surface gravity $\log g_2 = 8.73 \pm 0.05 \pm 0.05$ (statistical and systematic uncertainties, respectively), leading to a mass of $M_2 = 1.06\,\mathrm{M}_\odot$. The temperature of the extremely low-mass white dwarf (primary) is substantially lower at $T_1 = 6400 \pm 37 \pm 50$ K, while its surface gravity is poorly constrained by the data. The relative flux contribution of the two white dwarfs across the spectrum provides a radius ratio of $R_1/R_2 \simeq 4.2$, which, together with evolutionary models, allows us to calculate the cooling ages. The secondary massive white dwarf has a cooling age of $\sim$1 Gyr, while that of the primary low-mass white dwarf is likely to be much longer, possibly $\gtrsim$5 Gyr, depending on its mass and the strength of chemical diffusion. These results unexpectedly suggest that the low-mass white dwarf formed long before the massive white dwarf, a puzzling discovery which poses a paradox for binary evolution.

Key words: binaries: close – stars: individual: SDSS J125733.63+542850.5 – white dwarfs.

1 INTRODUCTION

Double white dwarf binaries are common end products of binary evolution (Marsh, Dhillon & Duck 1995; Toonen et al. 2014). Those with separations small enough to have experienced one or two common envelope phases are particularly interesting, as they are thought to be progenitors of supernovae Type Ia (Iben & Tutukov 1984; Webbink 1984), Type .Ia (Bildsten et al. 2007), R CrB stars (Webbink 1984) and AM CVn systems (Breedt et al. 2012; Kilic et al. 2014a). In addition, mergers of Galactic double white dwarfs occur relatively frequently (Badenes & Maoz 2012), and constitute the main source of the background gravitational wave signal at frequencies detectable from space (Nelemans, Yungelson & Portegies Zwart 2001; Hermes et al. 2012).

There is an important relation between the initial mass of a main-sequence star and the final mass of the white dwarf that will form the remnant of that star (Weidemann 2000). This initial-final mass relation predicts that extremely low-mass (ELM) white dwarfs, typically with masses $M_{\rm wd} \lesssim 0.3\,\mathrm{M}_\odot$, cannot yet form as a natural product of stellar evolution because the main-sequence lifetime of their low-mass progenitors is longer than the present age of our Galaxy. However, ELM white dwarfs can be formed in binary systems in which the separation is close enough for the two stars to interact significantly before the ELM progenitor has evolved off the main-sequence (mass transfer via Case A or early Case B Roche lobe overflow). The binary companion causes the evolution of the ELM progenitor to be truncated before ignition of helium, and after

⋆ E-mail: m.c.p.bours@warwick.ac.uk

ejection of the envelope the helium core is exposed as the ELM white dwarf. Typically, ELM white dwarfs have surface gravities $\log g < 7$, as well as relatively massive hydrogen envelopes ($\sim 10^{-3}$–10^{-2} $M_\odot$; Istrate et al. 2014b). New dedicated searches such as the ELM Survey have significantly increased the known population in recent years (Brown et al. 2010, 2012, 2013; Kilic et al. 2011, 2012). The majority of ELM white dwarfs are companions to other white dwarfs (Kaplan et al. 2014; this paper) or millisecond pulsars (see for example van Kerkwijk, Bergeron & Kulkarni 1996; Bassa et al. 2006; Antoniadis et al. 2013) and a few have been found in hierarchical triple systems (Kilic et al. 2014b, 2015; Ransom et al. 2014) or orbiting A- or F-type main-sequence stars (Breton et al. 2012; Maxted et al. 2014). The subject of this paper, SDSS J1257+5428, is a binary that likely belongs to the first of these classes, but, as we shall see, how it evolved into the system we see today is a mystery.

1.1 Introduction to SDSS J1257+5428

The double white dwarf binary SDSS J1257+5428 (full name: SDSS J125733.63+542850.5) was first discovered when the available Sloan Digital Sky Survey (SDSS; York et al. 2000; Eisenstein et al. 2006) subspectra were examined for radial velocity variations as part of the Sloan White dwArf Radial velocity Mining Survey (SWARMS; Badenes et al. 2009). Follow-up spectroscopy revealed radial velocity variations with a semi-amplitude of 323 km s^{-1}, which were interpreted to come from a 0.9 $M_\odot$ white dwarf. Combined with the orbital period of 4.6 h and the absence of additional spectral features, this suggested that the most likely companion would be a neutron star or a black hole (Badenes et al. 2009).

Follow-up *B*- and *R*-band spectroscopy revealed two distinct components in the spectra, although the Balmer absorption lines only showed a single sharp core (Kulkarni & van Kerkwijk 2010; Marsh et al. 2011). These deep, radial-velocity variable Balmer lines in fact originate in a cool, ELM white dwarf, which we hereafter refer to as the primary (because it dominates the flux at visual wavelengths, and following Kulkarni & van Kerkwijk 2010 and Marsh et al. 2011). The secondary is another white dwarf, which is hotter and significantly more massive, causing it to have very broad absorption lines. In addition, it is likely rotating fast, causing its line cores to be smeared out. Due to the shallow nature of these lines, and the absence of sharp cores, it was not possible to detect a radial velocity variation of the massive white dwarf.

The combination of these two white dwarfs in the same binary system is very interesting. The primary component is of much lower mass, and therefore has a much larger surface area than the secondary component. This causes the cooler primary to dominate the flux at wavelengths $\lambda \gtrsim 4000$ Å. At shorter wavelengths the secondary white dwarf starts dominating due to its higher temperature. Note that the fact that the higher mass white dwarf is hotter is contrary to expectation since it presumably formed much earlier than the low-mass white dwarf. At the time of the studies by Kulkarni & van Kerkwijk (2010) and Marsh et al. (2011) there were only a limited number of low-mass white dwarf models available, leaving it unclear whether or not the cool, low-mass white dwarf could have overtaken the secondary white dwarf on the cooling track. To securely measure the secondary's temperature, we have obtained *Hubble Space Telescope* (*HST*) far-ultraviolet spectra. These new measurements of the hot white dwarf are presented in this paper and combined with recent binary models for ELM helium white dwarfs (Althaus, Miller Bertolami & Córsico 2013; Istrate et al. 2014b) to study this binary's evolutionary history further.

2 OBSERVATIONAL DATA

2.1 The *HST* data

SDSS J1257+5428 was observed with the *HST* in Cycle 18, with programme ID 12207. Part of the observations were done with the Cosmic Origins Spectrograph (COS) on 2011 May 9, with the G140L grating and a central wavelength of $\lambda_{cen} = 1280$ Å. The total exposure time of these data is 146 min. The double white dwarf was also observed with the Space Telescope Imaging Spectrograph (STIS), on 2011 Oct 22. For these observations, totalling 95 min, the G230L grating was used at $\lambda_{cen} = 2376$ Å. The raw data were processed by the standard pipeline at the Space Telescope Science Institute.

In the following analysis we exclude parts of the *HST* spectra that are contaminated by geocoronal O I (1304 Å) emission. In addition, for the COS and STIS data, we have excluded data at wavelengths $\lambda > 1700$ Å and $\lambda < 1650$ Å, respectively, where the signal-to-noise ratio is very low. The measured flux is consistent with the *Swift* Ultra-Violet/Optical Telescope data presented in Marsh et al. (2011).

2.2 Parallax observations

We used the 2.4 m Hiltner telescope at the MDM Observatory on Kitt Peak on 19 observing runs between 2010 January and 2014 June. The astrometric solution includes 128 exposures, all taken in the *I* band. Observations, reductions, and analysis followed procedures similar to those described in Thorstensen (2003) and Thorstensen, Lépine & Shara (2008). The parallax of SDSS 1257+5428 relative to the reference stars was 8.3 mas, with a formal fitting error of only 0.8 mas, although we judged the external error to be 1.3 mas from the scatter of the reference stars. The colours and magnitudes of the reference stars yield a 1.6 mas correction due to the finite distance of the stars forming the reference frame, so our absolute parallax estimate is 9.9 ± 1.3 mas, which on face value gives a distance to SDSS J1257+5428 of $\sim 101 \pm 15$ pc. The proper motion relative to the reference frame is modest, $[\mu_X, \mu_Y] = [-45, +9]$ mas yr^{-1}; the PPMXL catalogue (Roeser, Demleitner & Schilbach 2010) gives $[-41.0, +11.8]$ mas yr^{-1}, in very good agreement. Thorstensen (2003) describes a Bayesian procedure for estimating a distance by combining parallax information with proper motion (interpreted using an assumed space–velocity distribution) and with photometric distances. For the present case, we used only the proper-motion constraint to avoid tautology. The small proper motion combines with the Lutz–Kelker correction to give an estimated distance of 112^{+20}_{-15} pc, slightly larger than the inverse of the parallax. Assuming a thick-disc velocity distribution increases this by another ~ 5 pc.

2.3 ULTRASPEC photometry

On the nights of 2015 March 2 and 3, we observed SDSS J1257+5428 with the high-speed photometric camera ULTRASPEC (Dhillon et al. 2014), which is mounted on the 2.4 metre Thai National Telescope located on Doi Inthanon, Thailand. In total, we obtained 240 min of g'-band data. The data were reduced using the ULTRACAM pipeline (Dhillon et al. 2007), with which we debiased and flatfielded the data and performed relative aperture photometry using a nearby bright star to minimize the effects of atmospheric variations in the light curves.

Table 1. White dwarf parameter results from the MCMC analysis performed on the *HST*+COS, *HST*+STIS and SDSS data. The reddening is constrained to $0 < E(B-V) < 0.0173$ by a uniform prior. Numbers in parentheses indicate statistical uncertainties in the last digit(s). The distance is calculated from the scale factor s (see Section 3 for details). The cooling ages τ_2 in each column are based on carbon/oxygen and oxygen/neon white dwarf models, with an estimated uncertainty of 0.1 Gyr.

Parameters	MCMC results	Best model (see Fig. 2)	MCMC (fixed log g_1)	MCMC (fixed log g_1)	MCMC (fixed log g_1)
T_2 (K)	13 030(70)	13 033	13 050(59)	12 965(82)	12 811(94)
T_1 (K)	6400(37)	6399	6402(38)	6395(29)	6460(24)
$E(B-V)$ (mag)	0.0089(34)	0.0101	0.0109(23)	0.0038(21)	0.0008(8)
$\log(g_2)$	8.73(5)	8.72	8.73(5)	8.70(7)	8.61(9)
$\log(g_1)$	5.26(36)	5.10	5.0	6.0	7.0
R_1/R_2	4.27(9)	4.27	4.29(9)	4.21(10)	3.89(9)
d (pc)	102(9)	103	102(9)	105(8)	109(8)
M_2 ($M_\odot$)	1.06(5)	1.05	1.06(5)	1.04(5)	1.00(5)
τ_2 (Gyr)	1.0 / 1.2	1.0 / 1.2	1.0 / 1.2	1.0 / 1.2	0.9 / 1.2
Details of the various fits					
minimum χ^2	5771(4)	5764	5771(4)	5774(4)	5817(4)
Degrees of freedom	11 071	11 071	11 072	11 072	11 072

3 FITTING SPECTRA USING A MARKOV CHAIN MONTE CARLO APPROACH

We fit both the *HST* COS and STIS spectra as well as the SDSS *ugriz* fluxes with a Markov Chain Monte Carlo (MCMC) analysis, using the affine-invariant ensemble sampler in the PYTHON package EMCEE (Foreman-Mackey et al. 2013). To obtain the SDSS fluxes, we use the PSF (point spread function) magnitudes, which we correct for the offset between the SDSS and AB magnitude systems using (−0.04, 0, 0, 0, 0.02) for the *ugriz* measurements, respectively.[1]

We fit the data with a sum of two white dwarf model spectra from Koester (2010), which employ a mixing length $\mathrm{ML2}/\alpha = 0.8$, and list the Eddington flux density at the surface of the white dwarf. The relative contribution of the two model spectra is determined by the radius ratio of the two white dwarfs. The MCMC method maximises the posterior probability, equivalent to minimizing χ^2, to find the best fit. Each data point is weighted by its uncertainty, with no additional weight in favour of either the *HST* or SDSS data.

The free parameters in our model are the temperatures T_1 and T_2, the surface gravities $\log g_1$, $\log g_2$, the radius ratio R_1/R_2, a scale factor $s = 4\pi R_1^2/d^2$ to account for the distance d to SDSS J1257+5428, and the maximum reddening along our line of sight $E(B-V)$, which is incorporated using the expressions presented in Seaton (1979) and Howarth (1983). We included a uniform prior on the reddening, constraining it to $0 < E(B-V)/\mathrm{mag} < 0.0173$, where the maximum is given by the dust map of Schlafly & Finkbeiner (2011) and we assume a minimum of zero. All other parameters are left unconstrained. We chose not to include a prior on the distance based on the parallax measurements, to allow a self-consistency check afterwards.

The results presented here are based on converged chains, from which the so-called burn-in phase is removed. We have also thinned the chains, by only storing each 20th model, in order to remove any correlation that may be present between subsequent models in the unthinned chain.

[1] http://www.sdss.org/dr12/algorithms/fluxcal/#SDSStoAB

4 RESULTS

For each of the free parameters, the mean value and 1σ uncertainty of the converged MCMC chain are listed in Table 1, column 2. Note that the quoted uncertainties are purely statistical. They do not include any systematic uncertainties that may be present, and are therefore underestimates of the true uncertainties. For our best model, the reduced $\chi^2 = \chi^2_\nu \simeq 0.5$. However, scaling the error bars on the data such that $\chi^2_\nu \simeq 1$ would only decrease the statistical uncertainties further, and we refrain from doing so. The results from our MCMC are shown in Fig. 1, projected on the various two-dimensional parameter planes, as well as in one-dimensional histograms. The best model, together with the *HST* and SDSS data, is shown in Fig. 2, and fits the data well at all wavelengths. The underpredictions of the model with respect to the *u* and *g* SDSS fluxes (shown in the bottom panel) are less than 3σ of the SDSS flux. Given that SDSS uncertainties do not include systematic uncertainties, we do not think this difference is significant.

4.1 The hot, massive white dwarf and possible pulsations

With an effective temperature of $T_2 = 13\,030 \pm 30$ K and a surface gravity of $\log g_2 = 8.73 \pm 0.05$, detailed evolutionary models show that the secondary star has a mass of $M_2 = 1.06 \pm 0.05\ \mathrm{M}_\odot$. The corresponding cooling age is $\tau_2 = 1.0$ Gyr or 1.2 Gyr, with an estimated uncertainty of 0.1 Gyr, for carbon/oxygen and oxygen/neon white dwarf models, respectively (Kowalski & Saumon 2006; Althaus et al. 2007; Tremblay, Bergeron & Gianninas 2011).[2] The values for the mass and surface gravity translate into a radius of $R_2 = 0.0074 \pm 0.0006\ \mathrm{R}_\odot$. These results are in agreement with those of Kulkarni & van Kerkwijk (2010), and the results of the fits to the phase resolved and ultraviolet–optical spectral energy distribution presented in Marsh et al. (2011).

At different composition-dependent epochs during a white dwarf's cooling process, the star experiences non-radial gravity-mode pulsations. The atmospheric parameters of the secondary white dwarf place it inside the empirical and theoretical instability strip for white dwarfs with hydrogen-rich atmospheres

[2] See http://www.astro.umontreal.ca/~bergeron/CoolingModels and http://fcaglp.fcaglp.unlp.edu.ar/evolgroup/

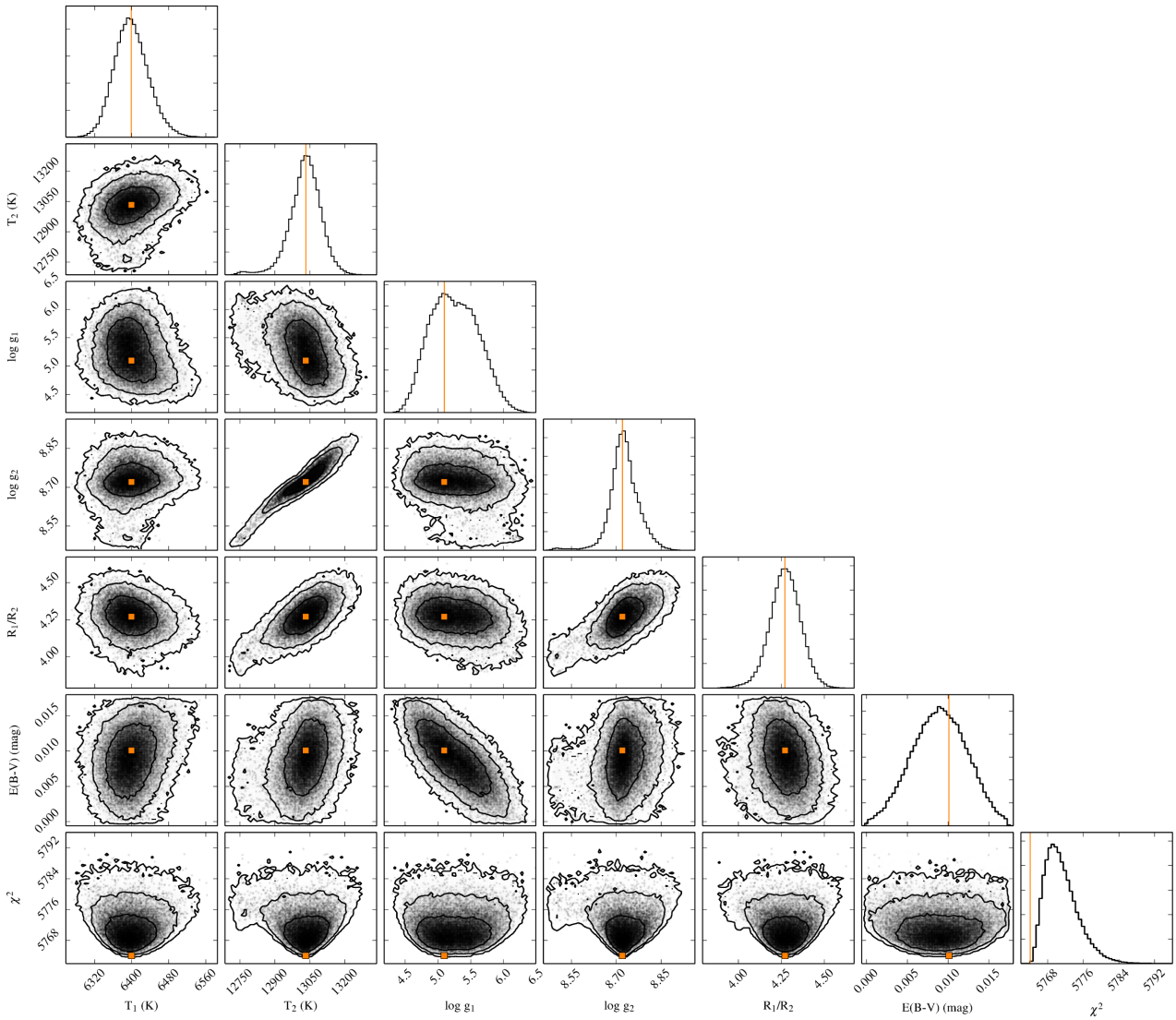

Figure 1. Converged MCMC chain projected on to two-dimensional parameter spaces and showing histograms for the individual free parameters in the fits. The contours are at the 1σ, 2σ and 3σ levels, and include 68 per cent, 95 per cent and 99.7 per cent of the data, respectively. The orange squares and vertical lines indicate the best-fitting model with $\chi^2 = 5764$, as listed in Table 1.

(Van Grootel et al. 2013; Gianninas et al. 2014b). At this high surface gravity, there are only two confirmed white dwarf pulsators (Gianninas, Bergeron & Ruiz 2011; Hermes et al. 2013). Note that this empirical instability strip is based on atmospheric parameters determined from Balmer line fits, in which the models used include a 1D mixing-length theory to approximate convective motion. The most recent models are based on 3D simulations instead, and give slightly different results for both white dwarf temperatures and surface gravities (Tremblay et al. 2013). Because our atmospheric parameters were not obtained through Balmer line fits, these do not suffer from inaccuracies in the 1D models. To facilitate direct comparison with the empirical instability strip, we therefore decided to 'correct' our results using the offsets from 3D to 1D parameters (Tremblay et al. 2013, $\Delta T \simeq 250$ K; $\Delta \log g \simeq 0.01$), rather than correcting every other source from 1D to 3D.

Although the secondary is placed ∼600 K from the blue edge inside the instability strip, we did not detect any pulsations in the time-tagged *HST* COS data down to an amplitude of 1.7 per cent, equivalent to 18 mmag at the 3σ limit. To bring this limit down, we obtained the ULTRASPEC data. However, these also do not show any pulsations with an amplitude exceeding 0.5 per cent. In the g'-band light curve the contribution of the secondary white dwarf is diluted by that of the primary, as the latter contributes 1.6 times as much flux at these wavelengths. This puts the 3σ pulsation amplitude limit at 14 mmag. Note that the *HST* limit is from data at far-ultraviolet wavelengths, where pulsation amplitudes are generally much larger than at optical wavelengths (Robinson et al. 1995), and may therefore still be the stronger limit even though the absolute value is somewhat higher than that from the ULTRASPEC data. Pulsation amplitudes tend to decline for white dwarfs with effective temperatures exceeding 11 500 K (Mukadam et al. 2006), and so it is possible that they are still present, but with amplitudes below the limits presented here.

4.2 The cool low-mass white dwarf

The secondary white dwarf mass determined above combined with the radial velocity variation of $K_1 = 330\,\mathrm{km\,s^{-1}}$ measured by Marsh

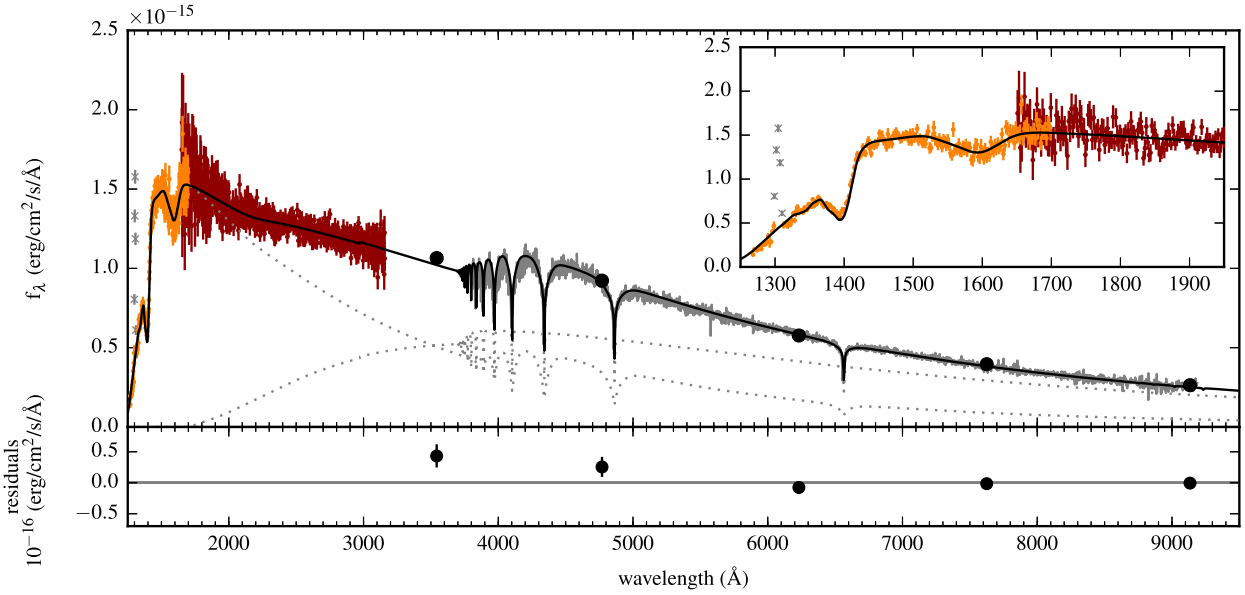

Figure 2. Top panel: best-fiting model spectra for the double white dwarf binary SDSS J1257+5428 (solid black line) and the individual white dwarfs (dotted grey lines). The *HST*+COS and STIS spectra are shown at $1200 < \lambda/\text{Å} < 1700$ and $1650 < \lambda/\text{Å} < 3200$, respectively, and are binned to 2 Å. Solid black dots indicate the SDSS *ugriz* fluxes (error bars too small to be seen). The inset shows a closer view of the far-UV, where the flux is almost entirely dominated by the hot white dwarf. The grey crosses indicate geocoronal oxygen emission ($\lambda \sim 1300$ Å), and are excluded from our fits. Bottom panel: residuals of the model SDSS J1257+5428 spectrum folded through the SDSS filter curves with respect to the measured SDSS fluxes.

et al. (2011) put an upper limit on the mass of the primary white dwarf at $M_1 \leq 0.24\,\mathrm{M}_\odot$ (see their fig. 6). This is consistent with the system not being a supernova Type Ia progenitor, as well as with the favoured solution found in Marsh et al. (2011).

One interesting result from our analysis is that the data strongly suggest that the surface gravity of the primary, cooler white dwarf is close to $\log g = 5.3$ (see Fig. 1). However, given the radius ratio of $R_1/R_2 = 4.27$ and a maximum possible mass ratio of $M_2/M_1 \simeq 10$, generously assuming a minimum white dwarf mass of 0.1 $\mathrm{M}_\odot$ (Althaus et al. 2013; Istrate, Tauris & Langer 2014a), the surface gravities can differ by $\log g_2 - \log g_1 \simeq 2.3$ at most. Given that the surface gravity of the hot white dwarf is well constrained by the features in the *HST*+COS data we therefore believe that the surface gravity of the cool white dwarf should be closer to $\log g_1 \sim 6.5$. In addition, there is no indication of any absorption lines besides the Balmer lines, even though at the very least the Ca H/K lines are often present in white dwarfs with $\log g \lesssim 6$ (Brown et al. 2013; Kaplan et al. 2013; Gianninas et al. 2014a; Hermes et al. 2014). This therefore also points towards a surface gravity larger than 5.3 for the low-mass white dwarf in SDSS J1257+5428. We do not know why the data imply the low surface gravity we find in an unconstrained fit. Considering the entire range of possible white dwarf surface gravities, a $\log g_1 \sim 6.5$ is still at the low end, and the combination with the low effective temperature is unprecedented, making it difficult to draw robust conclusions.

For these reasons, we reanalysed the data while keeping $\log g_1$ fixed, choosing values of 5.0, 6.0 and 7.0. The results are listed in the last three columns of Table 1. The large changes in $\log g_1$ have relatively little effect on the χ^2 value. The main difference between these results and those from our initial MCMC is in the values of the reddening and the radius ratio. The reddening decreases significantly, becoming consistent with zero when the primary white dwarf's surface gravity is fixed at higher values. This behaviour is likely caused by the near-ultraviolet feature in the interstellar extinction curve, which is adjusted to compensate for the change in the cool white dwarf's spectrum, which starts contributing to the total flux in this same wavelength range. The variation in the other parameters illustrates the extent of the systematic uncertainties, which are ∼150 K for T_2, ∼50 K for T_1 and ∼0.05 for $\log g_2$. Note that these uncertainties are too small to move the secondary out of the instability strip. The best fits from the three MCMC runs with fixed, different values of $\log g_1$ are shown in Fig. 3. Comparison of these models with the Balmer lines in the WHT+ISIS spectra presented in Marsh et al. (2011) shows that the model with $\log g_1 = 6.0$ matches the depths of those lines best, consistent with our reasoning above. From now on we therefore assume that $\log g_1 \simeq 6.0$–6.5, which agrees with the results from the unconstrained MCMC analysis at the $\sim 3\sigma$ level (see Fig. 1).

Given that the surface gravity of the cool white dwarf is poorly constrained by the spectra we do not rely on it hereafter, and instead use the radius derived for the hot, secondary white dwarf in Section 4.1, and the radius ratio from the MCMC analysis. The latter is constrained by the relative flux contributions of the two white dwarfs across the spectral energy distribution, and translates into a radius for the primary of $R_1 = 0.032 \pm 0.003\,\mathrm{R}_\odot$. In Fig. 4, we show this value and the effective temperature for the cool white dwarf, together with evolutionary models for white dwarfs of different mass from Istrate et al. (2014b). These models were obtained for ELM white dwarfs in close binaries with neutron stars, but we expect the white dwarf's formation via Roche lobe overflow and detachment to proceed similarly independent of the nature of the companion, apart from possible issues of mass-transfer instability. To avoid cluttering the figure, we only selected a few of the many models with various values of the initial mass of the donor star (the progenitor of the helium white dwarf), the index of magnetic braking, and the mass of the neutron star companion (see Istrate et al. 2014a for further

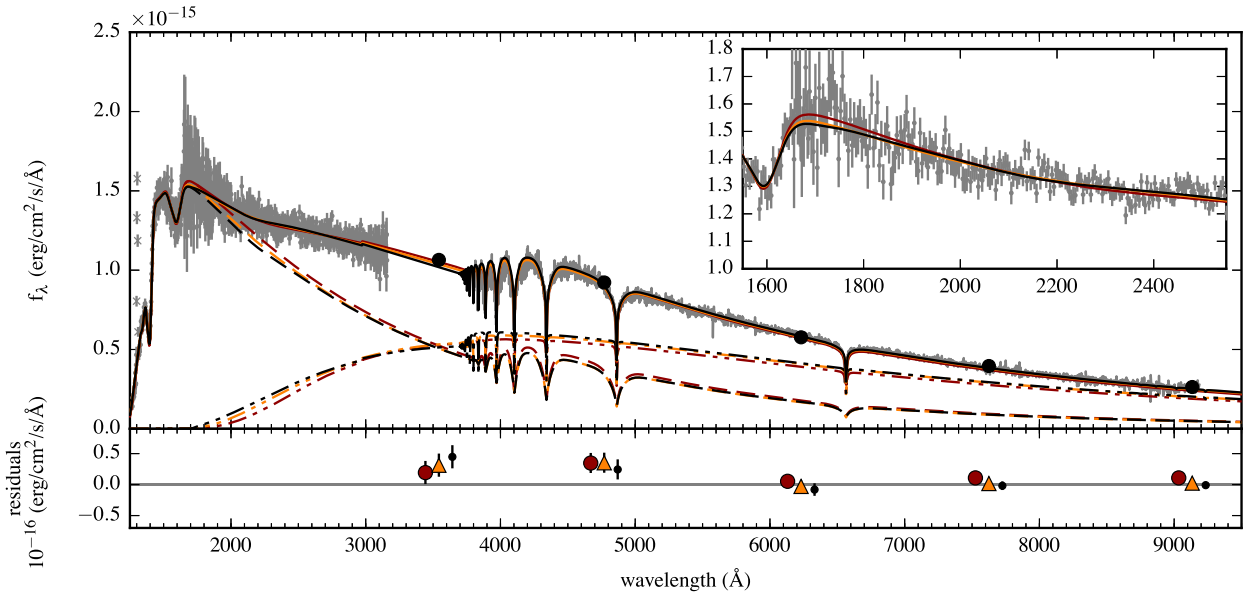

Figure 3. Top panel: best-fitting model spectra for the double white dwarf binary SDSS J1257+5428 (solid lines) and the individual white dwarfs (dashed and dot–dashed lines) from MCMC fits with log g_1 fixed at 5.0, 6.0 and 7.0 (black, orange and red, respectively). The *HST*+COS and STIS spectra (binned to 2 Å in the main panel, and 4 Å in the inset) and the SDSS spectrum are shown in grey. Solid black dots indicate the SDSS *ugriz* fluxes (error bars too small to be seen). The inset highlights the part of the spectrum where the models differ most. Bottom panel: residuals of the model SDSS J1257+5428 spectra folded through the SDSS filter curves with respect to the measured SDSS fluxes, offset by −100 Å, 0, +100 Å for log g_1 fixed at 7.0, 6.0 and 5.0, respectively.

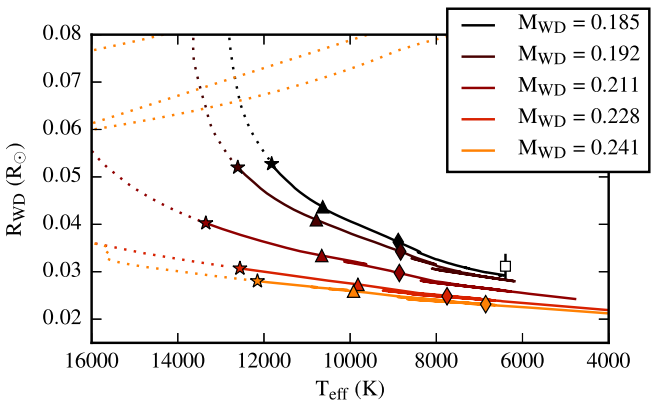

Figure 4. Cooling tracks for ELM white dwarfs, together with the radius and effective temperature of the cool low-mass white dwarf (open square). The lines are evolutionary models from Istrate et al. (2014b, see text for more details) for white dwarfs of different mass (in $M_\odot$, see legend). The various lines are dotted up to a cooling age of 1 Gyr (stars), and solid after. Triangles and diamonds are placed at cooling ages of 2.5 and 5 Gyr for each track. At $T_{\rm eff} = 6400$ K, the white dwarf cooling ages are roughly 13, 13, 10.5, 7.2 and 6.7 Gyr, with increasing mass, respectively.

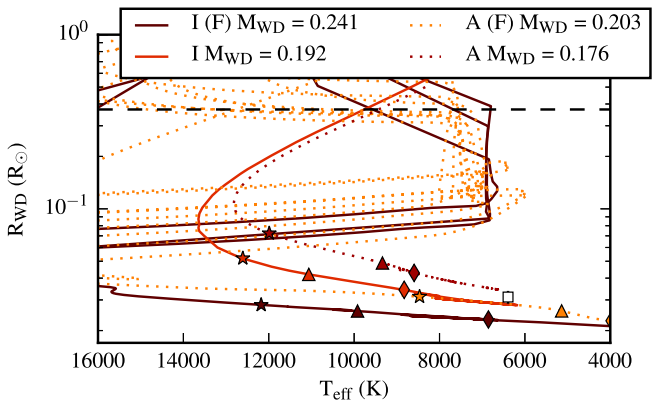

Figure 5. Cooling tracks for ELM white dwarfs, together with the radius and effective temperature of the cool low-mass white dwarf (square). The solid and dotted lines are evolutionary models from Istrate et al. (2014b, labelled I in the legend) and Althaus et al. (2013, labelled A), respectively. For each, a model with (labelled F) and without CNO flashes is included. The white dwarf masses are in $M_\odot$ as in the legend. The stars, triangles and diamonds indicate cooling ages of 1, 2.5 and 5 Gyr, respectively. The horizontal dashed line indicates the size of the ELM white dwarf's Roche lobe in the current binary configuration.

discussion). Our results indicate that the cool white dwarf has a low mass, close to 0.2 $M_\odot$, consistent with a low surface gravity. However, the models also show that such low-mass white dwarfs take ≥ 5 Gyr to cool to a temperature of 6400 K, much longer than the cooling age derived for the hot white dwarf, which is close to 1 Gyr. These values suggest, surprisingly, that the low-mass white dwarf formed first.

Fig. 5 shows a larger area of the same parameter space as shown in Fig. 4, now also including ELM white dwarf cooling models from Althaus et al. (2013). It is clear from this figure that the ELM white dwarf in SDSS J1257+5428 has settled on the cooling track and is not currently in a CNO flash cycle. Only ELM white dwarfs that exceed a certain mass experience CNO flashes, during which the thick hydrogen layer is quickly consumed, thereby speeding up the entire cooling process. Our upper limit of 0.24 $M_\odot$ is just above the minimum mass of 0.18 $M_\odot$ (Althaus et al. 2013) – 0.20 $M_\odot$ (Istrate et al. 2014b) necessary for cooling with CNO flashes.

As demonstrated in Figs 4 and 5, the age of the primary white dwarf estimated from current cooling models is very sensitive to both its mass and the degree of element diffusion. The shortest possible cooling age for the ELM white dwarf is given by a model from Althaus et al. (2013), in which the white dwarf is formed with a mass of 0.203 $M_\odot$, experiences CNO flashes, and takes

1.6 Gyr to reach a temperature of 6400 K. The difference in cooling ages between the Althaus et al. (2013) and Istrate et al. (2014b) models are most likely related to the amount of element diffusion (for example, via gravitational settling and radiative levitation; Althaus, Serenelli & Benvenuto 2001). The former models are calculated with gravitational settling, whereas the latter models do not include this effect. In addition, the treatment of convection may play a role. Finally, long-term helium white dwarf cooling (beyond the proto-white dwarf stage) could also be affected by rotation of the white dwarf, which might lead to significant mixing and thus prevention of strong element diffusion. New models investigating these issues are currently in progress (Istrate et al., in preparation).

The shorter cooling age of Althaus et al. (2013) is still too long to resolve the paradox of the formation of this binary. This is compounded by the time the ELM white dwarf took to form, since its progenitor most likely had a mass <1.6 M$_\odot$ (Istrate et al. 2014a), and thus had a main-sequence lifetime of the order of 1.5 Gyr (Hurley, Pols & Tout 2000), which needs to be added to the white dwarf cooling age to estimate its total age. Therefore, it appears impossible to avoid the conclusion that the ELM white dwarf is older than its massive white dwarf companion.

4.3 Distance to SDSS J1257+5428

Using the results for the scale factor, the radius ratio and the secondary radius from our MCMC analysis, we are able to calculate the distance via $d = R_1\sqrt{4\pi/s}$ for which we find $d = 105 \pm 8$ pc. This is consistent with the distance derived using parallax measurements, where $d = 112^{+20}_{-15}$ pc, as presented in Section 2.2, indicating that our analysis is sensible. At this point we could redo our analysis and include a prior on the distance, based on the parallax observations. However, given that the uncertainty on our current result is smaller than that from the parallax measurements, the prior would have little effect. Given furthermore that the scale factor s does not correlate significantly with any of the other free parameters, the values of these free parameters would change little and so we refrain from reanalysing the data.

5 DISCUSSION

The combined results of the *HST* data and evolutionary models for low-mass white dwarfs present us with an intriguing puzzle. The secondary white dwarf has a mass just over 1 M$_\odot$, which is near the threshold separating white dwarfs with a chemical core-composition of carbon/oxygen from those with oxygen/neon dominated cores (Lazarus et al. 2014). If it was an isolated star, we could use an initial–final mass relation to obtain an initial zero-age main-sequence mass of 5–6 M$_\odot$ (Catalán et al. 2008), for which main-sequence lifetimes are close to 100 Myr (Hurley et al. 2000). In close binaries the initial masses are often greater than those predicted from initial–final mass relations due to interactions between the stars, and so these numbers have to be considered cautiously. None the less, together with the cooling age of $\sim$1 Gyr, it allows us to estimate the total age of the hot, massive white dwarf as 1.1 ± 0.1 Gyr. The low temperature of the primary, low-mass white dwarf combined with evolutionary models shows that the age of the primary white dwarf is at least $\sim$1.6–5 Gyr. Given the 1.6 M$_\odot$ maximum progenitor mass, its total age is $\gtrsim$3 Gyr.

We considered whether the cooling age of the massive white dwarf could have been reset by accretion heating during the formation of the ELM white dwarf companion. However, this would imply that its cooling age would now be the same or longer (if only partially reset) than that of the ELM white dwarf, which does not explain what we see. There should be accretion after the birth of the ELM white dwarf during the CNO flashes as the white dwarf fills its Roche lobe (see Fig. 5). However, these events are very short lived ($\sim$100 yr) and cannot significantly alter the thermal structure of the massive white dwarf which takes $\sim 10^6$ yr to change (Bildsten et al. 2006).

A more exotic possibility is that the massive white dwarf formed out of a merger of two white dwarfs roughly 1 Gyr ago, and 4 Gyr after the formation of the ELM white dwarf. The pair had to form well before the ELM white dwarf and therefore survive at least 4 Gyr before merging. Considerations of dynamical stability (Eggleton, Fitchett & Tout 1989) show that if the outer period of this hypothetical triple matched today's 4.6 h period the inner period would have had to have been <1 h. This would result in a merger time-scale well short of the 4 Gyr minimum. Therefore, the triple scenario also requires shrinkage of the outermost orbit, which implies that the merger was a common-envelope event that shrunk both the inner binary and the outer binary/ELM white dwarf orbit. We cannot say whether this is impossible, but it seems unlikely; simulations of white dwarf mergers seem to show that the merged object does not expand significantly (Dan et al. 2011; Shen et al. 2012). If anything, one might expect that angular momentum from the merged pair would be transferred to the outermost orbit, resulting in a period increase, not the necessary decrease. Even if the proposed scenario is possible, it is hard to see how an initial configuration of a tight inner binary containing at least one carbon/oxygen white dwarf in a close triple with an ELM white dwarf could have formed.

Finally, it is possible that SDSS J1257+5428 is not a close double white dwarf, contrary to our assumption throughout the analysis presented here. As it has not been ruled out that the broad Balmer lines from the secondary massive white dwarf are stationary (Kulkarni & van Kerkwijk 2010; Marsh et al. 2011), the system could be a triple or the massive white dwarf could be aligned per chance with the ELM white dwarf binary instead. Perhaps the low-mass white dwarf is in a close binary with an unseen massive companion such as a neutron star, while the hotter, massive white dwarf is a wide companion. Recently, Ransom et al. (2014) discovered a triple system in the Galactic disc consisting of a neutron star and two white dwarfs, of which one is very low mass, and hence nature is apparently producing such triple compact star systems (Tauris & van den Heuvel 2014). However, in this scenario the problem with the incompatible cooling ages and masses remains, unless the hot white dwarf was captured as the third component later on and did not form at the same time as the close binary. Such an unusual scenario is only likely within a dense stellar cluster environment. Inspection of the *HST*+STIS acquisition image reveals that the PSF from the source is consistent with being a point source, and so the stars would have to be extremely well aligned if it was a chance alignment. This is also an argument against the system being a wide triple, although a close multiple system with a separation $\lesssim$10 au at the time of the observations cannot be ruled out.

Irrespective of the above possibilities, any binary or triple system, in which both of the observed white dwarfs discussed in this paper were formed, is difficult to reconcile with binary stellar evolution. This is mainly due to the fact that the progenitor star of the low-mass helium white dwarf most likely had a mass of 1–2 M$_\odot$ (Istrate et al. 2014a), and thus a much longer nuclear burning time-scale compared to that of the 5–6 M$_\odot$ progenitor of the $\sim$1 M$_\odot$ secondary massive white dwarf.

Future observations to clarify the nature of SDSS J1257+5428 could include radio observations to search for a neutron star

component, as well as phase-resolved spectroscopy to measure (or put an upper limit on) the radial velocity of the massive white dwarf. If such observations confirm the common binary nature of the two white dwarfs investigated here, we might be able to use their measured masses, radii and temperatures to constrain binary evolution and white dwarf cooling models further.

6 CONCLUSIONS

We have analysed the spectral energy distribution of the double white dwarf SDSS J1257+5428, consisting of *HST* COS and STIS data and *ugriz* flux measurements from SDSS. The effective temperature and surface gravity of the hot white dwarf are found to be $T_2 = 13\,030 \pm 70 \pm 150$ K and $\log g_2 = 8.73 \pm 0.05 \pm 0.05$. Evolutionary models show that this white dwarf has a mass of $M_2 = 1.06\,M_\odot$ and a cooling age of $\tau_2 \simeq 1$ Gyr. The atmospheric parameters place the star inside the ZZ Ceti instability strip, but we did not find any pulsations with amplitudes exceeding 18 mmag at far-ultraviolet wavelengths or 14 mmag in the optical g' band.

The temperature for the cool white dwarf is $T_1 = 6400 \pm 37 \pm 50$ K, while its surface gravity is constrained to $\log g_1 \sim 6.0$–6.5 by the radius ratio (in turn constrained by the relative flux contributions of the two white dwarfs), yielding a best mass estimate of $\leq 0.24\,M_\odot$, in agreement with Marsh et al. (2011). Using evolutionary models we find that the age must be > 3 Gyr, significantly longer than the 1.1 Gyr age of the hot white dwarf. The odd combination of both a higher temperature and a higher mass for the secondary white dwarf thus cannot be explained by substantial accretion during the time the primary white dwarf's progenitor evolved. The difference in cooling ages also rules out recent accretion-induced heating as the cause of the significant temperature difference between these two white dwarfs. Therefore the data surprisingly suggest that the low-mass progenitor of the primary white dwarf evolved before the high-mass progenitor of the secondary white dwarf, thus posing an interesting puzzle regarding their formation scenario.

ACKNOWLEDGEMENTS

We thank the referee for comments that helped improve the manuscript, and D. Townsley for useful discussions regarding the effect of accretion heating. The analysis presented in this paper is based on observations made with the NASA/ESA *HST*, obtained at the Space Telescope Science Institute, which is operated by the Association of Universities for Research in Astronomy, Inc., under NASA contract NAS 5-26555. These observations are associated with programme #12207. The research leading to these results has received funding from the European Research Council under the European Union's Seventh Framework Programme (FP/2007-2013)/ERC Grant Agreement no. 320964 (WDTracer). TRM and DS acknowledge financial support from STFC under grant number ST/L000733/1, and VSD under ST/J001589/1. MK gratefully acknowledges support of the NSF under grant AST-1312678, and JRT under AST-1008217.

REFERENCES

Althaus L. G., Serenelli A. M., Benvenuto O. G., 2001, MNRAS, 324, 617
Althaus L. G., García-Berro E., Isern J., Córsico A. H., Rohrmann R. D., 2007, A&A, 465, 249
Althaus L. G., Miller Bertolami M. M., Córsico A. H., 2013, A&A, 557, A19
Antoniadis J. et al., 2013, Science, 340, 448
Badenes C., Maoz D., 2012, ApJ, 749, L11
Badenes C., Mullally F., Thompson S. E., Lupton R. H., 2009, ApJ, 707, 971
Bassa C. G., van Kerkwijk M. H., Koester D., Verbunt F., 2006, A&A, 456, 295
Bildsten L., Townsley D. M., Deloye C. J., Nelemans G., 2006, ApJ, 640, 466
Bildsten L., Shen K. J., Weinberg N. N., Nelemans G., 2007, ApJ, 662, L95
Breedt E., Gänsicke B. T., Marsh T. R., Steeghs D., Drake A. J., Copperwheat C. M., 2012, MNRAS, 425, 2548
Breton R. P., Rappaport S. A., van Kerkwijk M. H., Carter J. A., 2012, ApJ, 748, 115
Brown W. R., Kilic M., Allende Prieto C., Kenyon S. J., 2010, ApJ, 723, 1072
Brown W. R., Kilic M., Allende Prieto C., Kenyon S. J., 2012, ApJ, 744, 142
Brown W. R., Kilic M., Allende Prieto C., Gianninas A., Kenyon S. J., 2013, ApJ, 769, 66
Catalán S., Isern J., García-Berro E., Ribas I., 2008, MNRAS, 387, 1693
Dan M., Rosswog S., Guillochon J., Ramirez-Ruiz E., 2011, ApJ, 737, 89
Dhillon V. S. et al., 2007, MNRAS, 378, 825
Dhillon V. S. et al., 2014, MNRAS, 444, 4009
Eggleton P. P., Fitchett M. J., Tout C. A., 1989, ApJ, 347, 998
Eisenstein D. J. et al., 2006, ApJS, 167, 40
Foreman-Mackey D., Hogg D. W., Lang D., Goodman J., 2013, PASP, 125, 306
Gianninas A., Bergeron P., Ruiz M. T., 2011, ApJ, 743, 138
Gianninas A., Hermes J. J., Brown W. R., Dufour P., Barber S. D., Kilic M., Kenyon S. J., Harrold S. T., 2014a, ApJ, 781, 104
Gianninas A., Dufour P., Kilic M., Brown W. R., Bergeron P., Hermes J. J., 2014b, ApJ, 794, 35
Hermes J. J. et al., 2012, ApJ, 757, L21
Hermes J. J., Kepler S. O., Castanheira B. G., Gianninas A., Winget D. E., Montgomery M. H., Brown W. R., Harrold S. T., 2013, ApJ, 771, L2
Hermes J. J. et al., 2014, MNRAS, 444, 1674
Howarth I. D., 1983, MNRAS, 203, 301
Hurley J. R., Pols O. R., Tout C. A., 2000, MNRAS, 315, 543
Iben I., Jr, Tutukov A. V., 1984, ApJS, 54, 335
Istrate A. G., Tauris T. M., Langer N., 2014a, A&A, 571, A45
Istrate A. G., Tauris T. M., Langer N., Antoniadis J., 2014b, A&A, 571, L3
Kaplan D. L., Bhalerao V. B., van Kerkwijk M. H., Koester D., Kulkarni S. R., Stovall K., 2013, ApJ, 765, 158
Kaplan D. L. et al., 2014, ApJ, 780, 167
Kilic M., Brown W. R., Allende Prieto C., Agüeros M. A., Heinke C., Kenyon S. J., 2011, ApJ, 727, 3
Kilic M., Brown W. R., Allende Prieto C., Kenyon S. J., Heinke C. O., Agüeros M. A., Kleinman S. J., 2012, ApJ, 751, 141
Kilic M. et al., 2014a, MNRAS, 438, L26
Kilic M., Brown W. R., Gianninas A., Hermes J. J., Allende Prieto C., Kenyon S. J., 2014b, MNRAS, 444, L1
Kilic M., Hermes J. J., Gianninas A., Brown W. R., 2015, MNRAS, 446, L26
Koester D., 2010, Mem. Soc. Astron. Ital., 81, 921
Kowalski P. M., Saumon D., 2006, ApJ, 651, L137
Kulkarni S. R., van Kerkwijk M. H., 2010, ApJ, 719, 1123
Lazarus P. et al., 2014, MNRAS, 437, 1485
Marsh T. R., Dhillon V. S., Duck S. R., 1995, MNRAS, 275, 828
Marsh T. R., Gänsicke B. T., Steeghs D., Southworth J., Koester D., Harris V., Merry L., 2011, ApJ, 736, 95
Maxted P. F. L. et al., 2014, MNRAS, 437, 1681
Mukadam A. S., Montgomery M. H., Winget D. E., Kepler S. O., Clemens J. C., 2006, ApJ, 640, 956
Nelemans G., Yungelson L. R., Portegies Zwart S. F., 2001, A&A, 375, 890

Ransom S. M. et al., 2014, Nature, 505, 520
Robinson E. L. et al., 1995, ApJ, 438, 908
Roeser S., Demleitner M., Schilbach E., 2010, AJ, 139, 2440
Schlafly E. F., Finkbeiner D. P., 2011, ApJ, 737, 103
Seaton M. J., 1979, MNRAS, 187, 73P
Shen K. J., Bildsten L., Kasen D., Quataert E., 2012, ApJ, 748, 35
Tauris T. M., van den Heuvel E. P. J., 2014, ApJ, 781, L13
Thorstensen J. R., 2003, AJ, 126, 3017
Thorstensen J. R., Lépine S., Shara M., 2008, AJ, 136, 2107
Toonen S., Claeys J. S. W., Mennekens N., Ruiter A. J., 2014, A&A, 562, A14
Tremblay P.-E., Bergeron P., Gianninas A., 2011, ApJ, 730, 128
Tremblay P.-E., Ludwig H.-G., Steffen M., Freytag B., 2013, A&A, 559, A104
Van Grootel V., Fontaine G., Brassard P., Dupret M.-A., 2013, ApJ, 762, 57
van Kerkwijk M. H., Bergeron P., Kulkarni S. R., 1996, ApJ, 467, L89
Webbink R. F., 1984, ApJ, 277, 355
Weidemann V., 2000, A&A, 363, 647
York D. G. et al., 2000, AJ, 120, 1579

This paper has been typeset from a TEX/LATEX file prepared by the author.